Biomaterials 31 (2010) 3422–3428

Contents lists available at ScienceDirect

Biomaterials

journal homepage: www.elsevier.com/locate/biomaterials

Cell-laden microwells for the study of multicellularity in lymphocyte fate decisions

Junsang Doh [a,b,*], Miju Kim [a], Matthew F. Krummel [c,**]

[a] School of Interdisciplinary Bioscience and Bioengineering, Pohang University of Science and Technology, San31, Hyoja-dong, Nam-Gu, Pohang, Gyeongbuk 790-784, Republic of Korea
[b] Department of Mechanical Engineering, Pohang University of Science and Technology, San31, Hyoja-dong, Nam-Gu, Pohang, Gyeongbuk 790-784, Republic of Korea
[c] Department of Pathology and Biological Imaging Development Center, University of California San Francisco, 513 Parnassus Ave, HSW-512, San Francisco, CA 94143-0511, USA

ARTICLE INFO

Article history:
Received 8 December 2009
Accepted 7 January 2010
Available online 1 February 2010

Keywords:
Hydrogel microwell
Multicellularity
T cell
Fate decision

ABSTRACT

Cell–cell cooperativity in populations of motile and transiently interacting immune cells has been difficult to assess in the absence of tools to control proximity and communication. Here, we describe the generation of cell-laden microwells that can precisely control contact-mediated interactions and multicellular 'quorum' decisions in lymphocytes. Different types of fate decisions for activating T cells can be shown to variously obey 'binary' or 'density' outcomes, correlated with cell–cell contact, using this new platform.

1. Introduction

Recent advances in microfabrication-based cell culture systems [1] have been crucial in establishing the role of multicellular interactions on many biological processes in multicellular organisms such as differentiation [2,3], proliferation [4,5], morphogenesis [6], cellular functions [7] by allowing precise control of either contact-dependent cell–cell communication [8] or multicellular aggregate size [9,10]. While multicellularity of many different cell types including embryonic stem cells [3], neural stem cells [2], hepatocytes/fibroblasts [7], and endothelial cells [4] has been examined, multicellular interactions among immune cells, which have distinct characteristics such as high motility and weak adhesiveness, have not been considered.

Optimal immune responses against foreign invaders with minimal damages on self require coordinated collaboration of many immune cells. Unlike stromal or epithelial cells residing in specific locations of tissues or organs, immune cells actively migrate tissues and organs [11,12], thus complex multicellular cooperation among immune cells have only recently become accessible by such methods as two-photon microscopy [13]. Multicellular clusters of immune cells have been described in vivo [14–16], but the functional importance of such multi-body interactions in regulating specific avenues of communication has been elusive mostly due to lack of tools to systematically manipulate multicellular interactions of weakly adhering immune cells. Here, we have demonstrated that cell-laden hydrogel microwells can be used to study the role of multicellularity on fate decisions such as cell-cycle progression and apoptosis in lymphocytes.

2. Materials and methods

2.1. T cell preparation

$CD4^+$ T cells were isolated from spleens and lymph nodes of C57BL/6 mice (Jackson Lab, All mice were maintained in accordance with the guidelines of the Lab Animal Resource Center of the University of California, San Francisco.) using a $CD4^+$ negative selection StemSep purification kit (Stem Cell Technologies, Inc.). Purified $CD4^+$ T cells were activated by plate-bound anti-CD3 (UCSF hybridoma core, clone: 2C11) and anti-CD28 (UCSF hybridoma core, clone: PV1). 24 well plates were coated with 1 μg/ml of anti-CD3 and 1 μg/ml of anti-CD28 in PBS for 1 h at 37 °C, and two million purified $CD4^+$ T cells in 1 ml of complete RPMI media (RPMI 1640 with 10% FCS, 2 mM L-Glutamine, 100 units/ml of penicillin, 100 mg/ml of streptomycin, and 50 mM β-mercaptoethanol) were plated in the anti-CD3/CD28 coated plates and incubated at 37 °C with 5% CO_2. After 16 h of anti-CD3/CD28 stimulation, activating T cells were harvested from the plates. Dead cells during stimulation were removed using Histopaque 1077 (Sigma–Aldrich), and live cells were kept in ice for T cell array fabrication (typically less than an hour).

2.2. Flow cytometry analysis of T cell proliferation and apoptosis

$CD4^+$ T cells purified from C57BL/6 mice were labeled with 1 μM of carboxyfluorescein diacetate, succinimidyl ester (CFSE, Invitrogen). Upon cell division, CFSE

* Corresponding author. San31, Hyoja-dong, Nam-Gu, Pohang, Gyeongbuk 790-784, Republic of Korea. Tel.: +82 54 279 2189; fax: +82 54 279 3199.
** Corresponding author. Tel.: +1 415 514 3130; fax: +1 415 514 3165.
E-mail addresses: jsdoh@postech.ac.kr (J. Doh), matthew.krummel@ucsf.edu (M.F. Krummel).

0142-9612/$ – see front matter © 2010 Elsevier Ltd. All rights reserved.
doi:10.1016/j.biomaterials.2010.01.018

in the cytoplasm of mother cells are equally divided into daughter cells, thus the fluorescence intensities of daughter cells are half of those of mother cells. Changes in fluorescence intensities by cell division can be quantitatively monitored by flow cytometry and systematically tracked [17]. CFSE-labeled $CD4^+$ T cells were activated by plate-bound anti-CD3/anti-CD28 for 16 h, washed twice, and re-plated on uncoated plates with three-fold serial dilution. Proliferation and survival of re-plated T cells were assayed by flow cytometry (FACS Calibur, BD Biosciences) using CFSE dilution and propidium iodide (PI) stain, respectively, 24 h after re-plating.

2.3. Measurement of T cell sizes

Naïve $CD4^+$ T cells were purified from C57BL/6 mice and labeled with CFSE. Activated $CD4^+$ T cells were prepared by stimulating CFSE-labeled naïve $CD4^+$ T cells with plate-bound anti-CD3/anti-CD28 for 16 h. Two different concentrations of anti-CD3 and anti-CD28 solutions (1 μg/ml of each antibody and 10 μg/ml of each antibody) were used to coat plates for T cell stimulation. T cells were stained with allophycocyanin (APC) conjugated anti-CD4, stored in ice for 30 min, placed in 8 well Labtek chamber (Nunc) with DAPI, and imaged immediately. Differential Interference Contrast (DIC)/DAPI/CFSE/APC images were obtained, and only $DAPI^-CD4^+$ cells were used for size measurement. CFSE images were used to measure the area of T cells, and diameter was calculated from the area measured.

2.4. PDMS mold fabrication

Micropatterned silicon masters were fabricated at Stanford Nanofabrication Facility (SNF) by standard photolithography using 7 μm thick SPR-200-7 (Shipley) positive photoresist films on silicon wafer. Sylgard 184 pre-polymer base and curing agent (Dow chemical) were casted onto the positive photoresist patterned silicon masters, cured 24 h at room temperature. Then, cured PDMS were gently peeled off (Fig. 1B(i)), and cut to create open channels.

2.5. T cell-laden hydrogel microwell fabrication

All chemicals were from Sigma–Aldrich and used as received unless otherwise noted. Microwells were fabricated in glass bottom petri dishes (MatTek Corporation, 35 mm petri dish with a 14 mm No. 1.5 glass window) in a similar way as described elsewhere (Fig. 1) [18]. Firstly, glass surfaces were functionalized with biotin and acrylate groups as schematically shown in Fig. 1A. Briefly, glass bottom of the dishes were cleaned 10 M NaOH and amine groups were introduced to the glass surfaces by immersing cleaned glasses in 1 wt% solution of 3-aminopropyl triethoxysilane in sodium acetate buffer (100 mM, pH 4.5) for 30 min (Fig. 1A(i)). Then, amine-functionalized dishes were baked at 90 °C for 2 h under vacuum for curing, further functionalized by overnight incubation in PBS solution containing 2 mM of Biotinamidohexanoic acid N-hydroxysuccinimide ester (Biotin-LC-NHS) and 0.2 mM of acrylic acid N-hydroxysuccinimide ester (acrylate-NHS) (Fig. 1A(ii)), and dried by air blowing. Glasses with dual functionality were essential for the microwell fabrication; biomolecules and cells can be attached by biotin-group via biotin–streptavidin bridges and hydrogel microwell can be stably attached on the glasses by acryl group by co-polymerization of acryl group during photo-polymerization. Secondly, hydrogel microwells were created on the dual-functionalized glass surfaces (Fig. 1B(ii)). Hydrogel precursors were prepared by dissolving 20% (v/v) poly (ethylene glycol) dimethacrylate (PEGDMA, Mn ~ 750 Da) and 1% (w/v) hexyl phenyl ketone (HPK) in 70/30 ethanol/water mixture, and purging with nitrogen for 10 min. PDMS molds were placed on the functionalized glass substrates and hydrogel precursor solution was perfused into the open channel formed between PDMS mold and functionalized glasses and polymerized by UV irradiation (Fig. 1B(ii)). By gently peeling off PDMS mold from the substrates, hydrogel microwells were obtained. Thirdly, the floors of the hydrogel microwells were coated with a capturing antibody by adsorbing streptavidin (Invitrogen, 10 μg/ml in PBS for 30 min) and subsequently adsorbing biotinylated anti-CD44 (made in house from hybridoma IM7, 5 μg/ml in PBS) (Fig. 1B(iii)). Fourthly, we applied 200 μl suspensions of activating T cells (2×10^7 cells/ml) in the anti-CD44 functionalized dishes and incubated at 4 °C for 1 h with gentle shaking. Then, by gently washing cell-seeded dishes with cold PBS, we

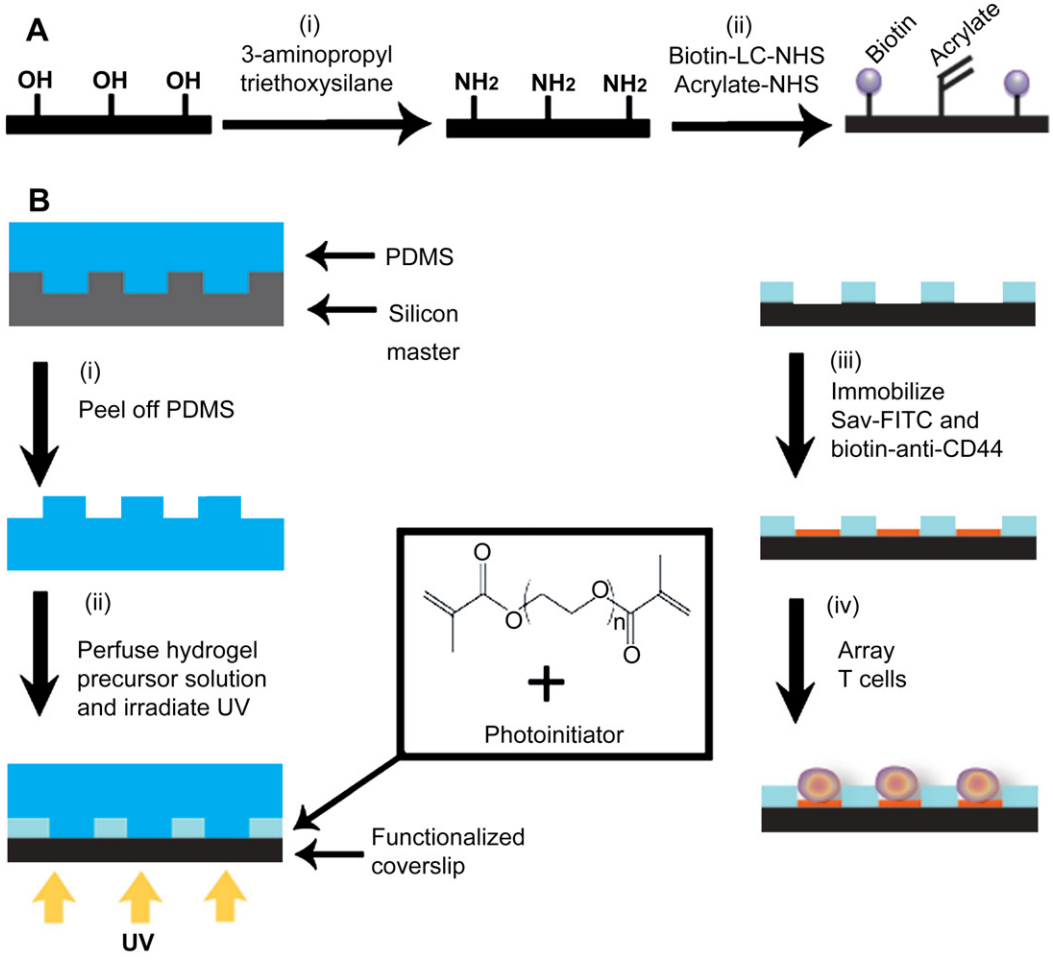

Fig. 1. Schematics of T cell-laden hydrogel microwell fabrication. A. Schematic procedure of glass functionalization. B. Schematic procedure of T cell-laden hydrogel microwell fabrication.

could remove non-adhering and weakly adhering cells by non-specific interactions, resulting in cellular arrays of T cells in hydrogel microwells (Fig. 1B(iv)).

2.6. DAPI and Ki-67 staining of T cells in microwells

T cell-laden microwells were incubated at 37 °C with 5% of CO_2 for 12 h to let T cells in the microwells interact with each other. Then, nuclei of dead cells were stained with DAPI at 4 °C for 10 min. After washing three times with cold PBS to completely remove DAPI in the media, cells were fixed with 2% paraformaldehyde (PFA) for 15 min at room temperature (r.t.), permeabilized with 0.2% saponin, and stained with anti-Ki-67 (BD Biosciences, Clone: B56) for 30 min at r.t. and polyclonal rhodamine-conjugated anti-mouse antibody (Jackson immunoresearch) for 30 min at r.t.

2.7. Fluorescence microscopy and data analysis

A modified Zeiss Axiovert 200 M microscope with a plan-neofluar 40X objective (Carl Zeiss, Inc.) was used for imaging experiments. The microscope was fitted with dual excitation and emission filter wheels and a Photometrics Coolsnap-HQ camera (Roper). Metamorph (Universal Imaging, Molecular Devices, Corp.) was used for image acquisition and analysis. DIC and DAPI/red fluorescence images were acquired for the fixed and stained cells in the microwells. Fluorescence images were acquired by optical sectioning (25 individual planes, 0.5 μm apart) and analyzed by integrating fluorescence intensities all the acquired planes into a single plane. Total number of cells in the microwells and DAPI and Ki-67 cells were manually counted.

3. Results and discussion

Activating murine $CD4^+$ T cells were used as a model system. Evidence that activating T cells determine their fate via direct cell–cell contacts initially came from adjusting the density of $CD4^+$ T cells in bulk media, followed by tracking their fates by flow cytometry. We purified $CD4^+$ T cells from wild type C57BL/6 mice, labeled them with carboxyfluorescein diacetate succinimidyl ester (CFSE), a fluorescence dye for tracking proliferation of cells [17], activated them with plate-bound anti-CD3/anti-CD28 for 16 h, harvested and re-plated to uncoated 96 well plates with serial dilution. After 24 h of re-plating, cell fates were analyzed by flow cytometry. As cell concentration decreases, the size and the number of clusters decreased (data not shown), and more cell death and less proliferation occurred (Fig. 2). However, in this setting, it was impossible to distinguish whether decrease in the survival and proliferation of cells in more diluted samples was due to reduced multicellular clustering or dilution of soluble factors secreted by T cells. In order to dissect the role of close-range communication on the fate decision of T cells, degree of clustering must be varied while all the other cellular environments are fixed. Also, analysis should be performed under conditions that conserve already-formed cellular clusters.

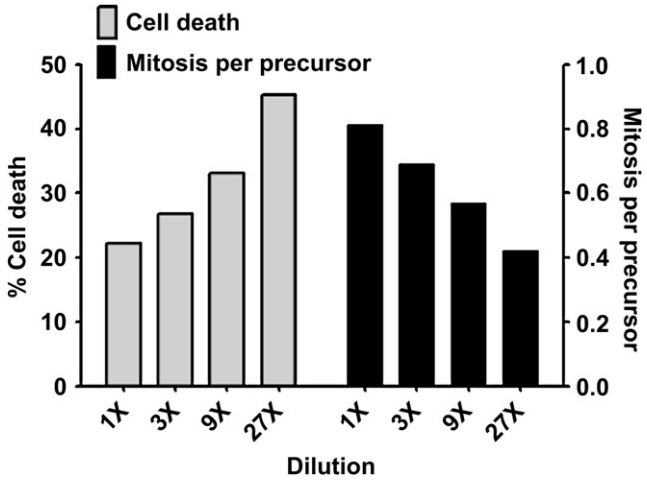

Fig. 2. Effect of cell density on survival and proliferation of activating T cells. Data is representative of three independent experiments.

To satisfy these requirements, we devised experimental settings based on cell-laden microwells as schematically shown in Fig. 3A. By varying the size of microwells, we can generate single cell arrays as well as arrays accepting multicellular clusters composed of different number of cells. This type of lymphocyte-laden microwells has been successfully used for single cell based assays [18–20], but has not been used for the study of multicellular interactions. The effect of cluster size can be investigated by comparing cells in different sizes of 'social' microwells, where the degree of multicelluarity is controlled by the dimensions of the microwells. The absolute effect of cell–cell contact can be assessed by comparing cells in social microwells and cells in a cluster of 'lonesome' microwells, where each microwell contains only one cell. In this way, contact-dependent signaling interactions can be controlled independently from cell density. Also, by fabricating different sizes of microwells in the same plates, all the cells in the different sizes of microwells will be under the same bulk media, thus only local microenvironments will be varied. To determine the size of 'lonesome' microwells, the diameter of T cells at 4 °C, the temperature at which T cells will be plated into the microwells, were measured by microscopy. During activation, the size of T cells

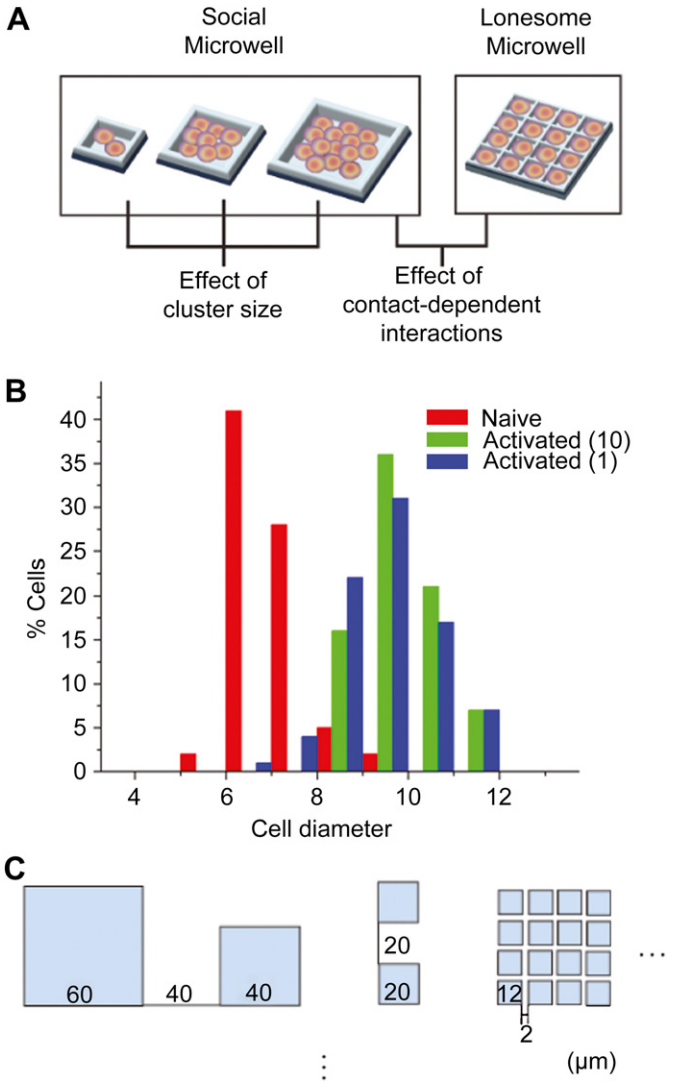

Fig. 3. Design of a microwell-based assay system for the assessment of multicellularity of T cells. A. Control of multicellular interactions using various sizes of microwells. B. Size distribution of naïve and activating T cells. C. Layout of microwell arrays.

increased depending on the strength of stimulation; the average diameter of T cells increased ~33% (by 7.1–9.5 μm) when naïve T cells were stimulated for 18 h with plate-bound anti-CD3 and anti-CD28 (1 μg/ml each), and the average diameter became slightly greater (9.8 μm) when higher concentration of anti-CD3 and anti-CD28 (10 μg/ml) were used (Fig. 3B). However, the maximum diameter of T cells was always less than 12 μm regardless of the stimulation strength, and thus we established 'lonesome' microwells at 12 μm maximal dimensions. This is an important parameter; if the size of lonesome microwell is too large, most of the lonesome microwells will be occupied by more than two T cells. If the size of lonesome microwell is too small, lonesome microwells will be preferentially occupied with poorly activated T cells. While these arrays may not fully recapitulate the 3-D environments of a lymph node, they nevertheless provide a framework for comparing activation in the presence or absence of cell–cell contact, focusing specifically on T–T interactions. For social microwells, we selected three different sizes, 20 μm, 40 μm, and 60 μm; activating T cells in priming lymph nodes forms diverse sizes of multicellular clusters ranging from doublets to several tens of micrometers in diameter [15]. Arrays of microwells were designed as schematically shown in Fig. 3C. A base unit of microwell arrays consists of one 60 μm, one 40 μm, and two 20 μm social microwells and 4 × 4 clusters of lonesome microwells. Distance between each social microwell or lonesome microwell cluster was set to 40 μm to have four sets of microwells in the field of view of microscope (160 μm × 200 μm) with 40× objective lens for facile data acquisition and analysis while maintaining sufficient distances to minimize diffusion based crosstalk. The distance between lonesome microwell in lonesome microwell clusters was set to 2 μm, a minimal width to support the structure of microwell, to allow neighboring T cells communicate by soluble factors while their contact-dependent interactions are completely blocked.

T cell-laden hydrogel microwells were fabricated by following the procedure schematically shown in Fig. 1 [18]. Firstly, glass coverslips attached at the bottom of the MatTek dishes were functionalized with biotin and acrylate by the scheme shown in Fig. 1A. Substrates with dual functionality were essential for the microwell fabrication; biomolecules and cells can be attached by biotin-group via biotin–streptavidin bridges and hydrogel microwell can be stably attached on the glasses by acryl group by co-polymerization of acryl group during photo-polymerization. Then, poly(dimethyl siloxane) (PDMS) molds made by casting Sylgard 184 mixture on a patterned silicon master (Fig. 1B(i)) were brought into tight contact with dual-functionalized glass coverslips. Poly(ethylene glycol) (PEG) hydrogel precursors were perfused into the channel formed between functionalized coverslips and PDMS molds by capillary force, and cured by UV irradiation (Fig. 1B(ii)). After curing, PDMS molds were gently removed, and FITC-labeled streptavidin (SAv-FITC) and biotinylated anti-CD44 were sequentially immobilized on the floors of PEG hydrogel microwells (Fig. 1B(iii)). It has been previously shown that anti-CD44 can immobilize T cells without perturbing biological functions of T cells [18]. Since PEG hydrogel prevented non-specific adsorption of proteins [18], SAv-FITC signal was only detected at the floors of the microwells when we examined with fluorescence microscopy (Supplementary Information (SI) Fig. S1). Finally, activating T cells were seeded on the anti-CD44 functionalized microwells. T cells were selectively captured in the microwells. By gently rinsing non-adhering T cells, T cell-laden microwells were fabricated (Fig. 1B(iv)).

Successfully fabricated hydrogel microwells and T cell-containing microwells are shown in Fig. 4A and B, respectively. The number of T cells per microwells was proportional to the size of microwells for social microwells as shown in Fig. 4C. Most of lonesome microwells (1050 out of 1120) were occupied by T cells, and more than 90% of T cells in lonesome microwells were singlets. Also, the majority of 4 × 4 clusters were occupied by more than 14 cells. Together, T cell-laden microwells that could precisely control size of multicellular clusters and cell–cell contact were successfully fabricated. Three-dimensional cellular cluster fabrication techniques previous used for stem cell studies cannot be applied for this case because stable 3-D cellular cluster formation typically takes several hours to a day [2,3,10], while activating T cell fate decisions that we aimed to study happens within 12 h.

Having provided a framework for quantitatively controlling cell–cell contact based communication, we applied this to analyzing viability and cell-cycle entry by plating activation cultures following a 16 h period in bulk culture with anti-CD3/CD28. This procedure, Fig. 5A, mimics the sequence of events occurring in vivo; homotypic T cell cluster formation in situ was not observed prior to an obligate activation stimulation through the T cell receptor (Fig. S2 in SI) [15]. Subsequently, the fate of T cells in the microwells was analyzed by fluorescence microscopy. Survival of the T cells was assessed by DAPI staining, which specifically stains nuclei of dead cells [21–23]. Simultaneously, cell-cycle entry in T cells was measured by staining Ki-67, a marker in all the cell cycles (G1, S, G2, and M) except G0 phase [24]. Early assessment of proliferation is essential in this setting since massive cell division may cause overflow of microwells. Indeed, a substantial fraction of activating T cells expressed Ki-67 before their first division (~16% of T cells at 24 h after activation) when we characterized expression dynamics of Ki-67 and its correlation with subsequent cell division by flow cytometry (Fig. S3 in the SI). When we performed the DAPI and Ki-67 staining right after plating T cells into microwells, less than 2% of T cells (8 out of 512) was stained with DAPI, and no Ki-67+ cells were observed, indicating perturbation of cells during the microwell plating step is minimal. With this flat baseline, we then assessed cell death and cell-cycle entry of activating T cells in microwells 12 h after plating. Fig. 5B presents representative pictures of DAPI and Ki-67 staining of T cells in various sizes of microwells. Percentages of DAPI-stained cells and Ki-67-positive cells in each size of microwell were plotted in Fig. 5C. For lonesome microwells, only singlets of T cells were counted.

About two-fold higher rate of cell death was observed for T cells in lonesome microwells compared to T cells in social microwells, and the rates of cell death in social microwells were almost identical regardless of the well size. In contrast, proliferation of T cells gradually increased as the size of microwells increased. These trends are quite different from those obtained by bulk experiment using serial dilution (Fig. 2) where both survival and proliferation were diminished over dilution. It still needs to be determined whether this discrepancy might simply reflect differences in dimensionality (we used 2-D cellular aggregates while 3-D cellular aggregates were formed in bulk serial dilution experiments); there are evidences that cells in 3-D behave quite differently from cells in 2-D [1,25]. However, by fabricating lymphocyte-laden microwells, we could systematically investigate the role of contact-dependent interactions as well as multicellular cluster sizes under identical bulk-media conditions, which are major focuses of the current study. These factors cannot be manipulated systematically and independently by the conventional bulk dilution assays.

Increased cell death and decreased proliferation in lonesome microwell might be due to some adverse effect of microwell walls. To rule out this possibility, we compared cell viability and cell-cycle entry of T cells in contact with 60 μm microwells and T cells in the center region of the microwells in the identical social microwells (Fig. 5D). We observed similar level of cell death regardless of the position of T cells in the social microwell,

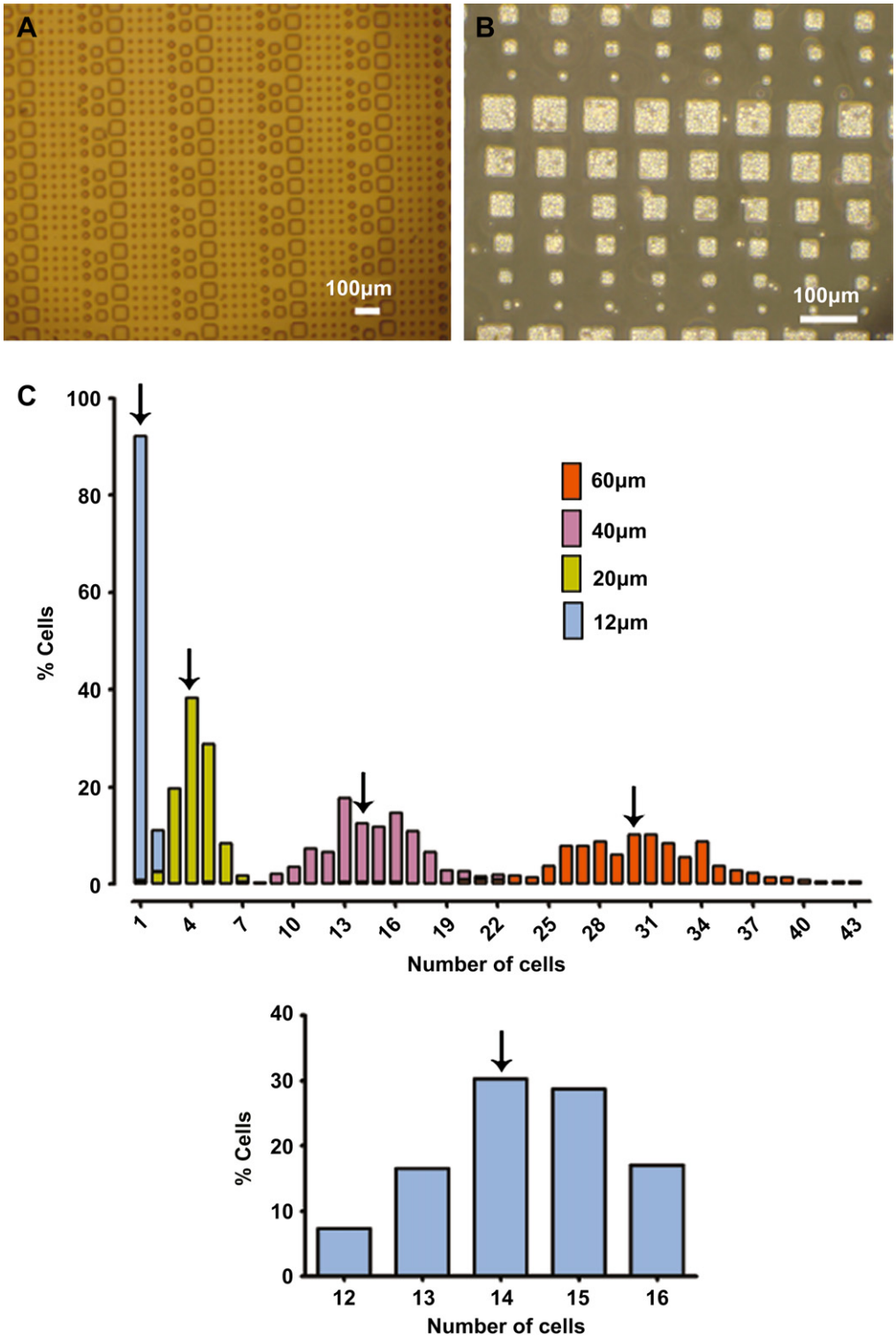

Fig. 4. Fabrication and characterization of T cell-laden hydrogel microwell arrays. A. Low magnification optical micrograph of fabricated hydrogel microwells with various sizes (12 μm, 20 μm, 40 μm, and 60 μm). B. Low magnification optical micrograph of T cell-laden microwell with various sizes (12 μm, 20 μm, 40 μm, and 80 μm). C. Cell number distributions of microwells with different sizes (12 μm, 20 μm, 40 μm, and 60 μm). Average values are indicated by arrows. D. Cell number distribution of a 4 × 4 cluster of lonesome microwells. An arrow indicates an average.

suggesting enhanced cell death in 'lonesome' microwell is due to lack of cell–cell contact not due to some cytotoxic effect of microwells. Interestingly, T cells in the center of social microwells exhibited higher rate of proliferation than T cells at the edge of social microwells, potentially due to enhanced cell–cell contact at the center region.

These results suggest that proliferation and cell death are independently controlled using 'binary' or 'density' measures of

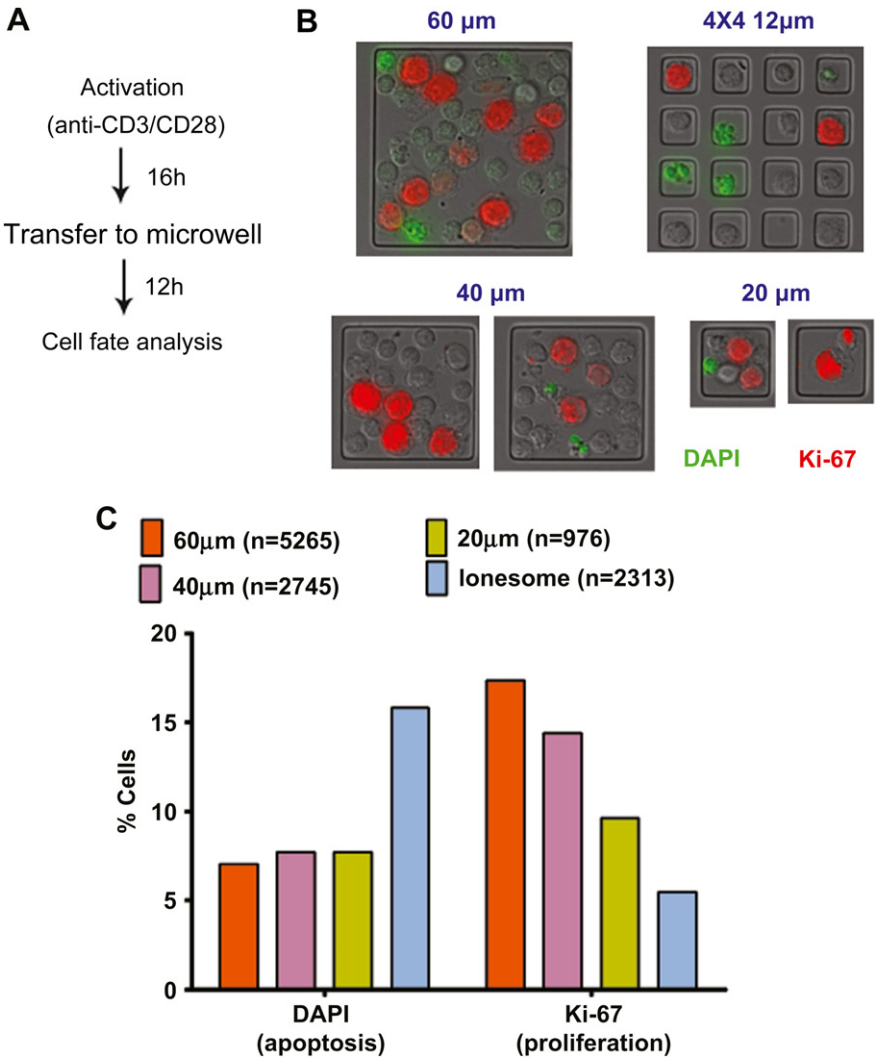

Fig. 5. Cell fate analysis of T cells in microwells. A. Schematic of experimental procedure. B. Representative DIC/DAPI/Ki-67 overlay images of various sizes of microwells. C. Percentages of $DAPI^+$ or $Ki\text{-}67^+$ T cells in the various sizes of microwells. Data is representative of three independent experiments. D. Position dependence of $DAPI^+$ or $Ki\text{-}67^+$ T cells in 60 μm social wells.

surrounding cells. On the one hand, any degree of contact-dependent interaction between activating T cells is sufficient to minimize cell death that rises when single cells are observed. In contrast, a 'density' measure appears more important for cell proliferation as T cells in varying density social microwells exhibited identical level of apoptosis, but quorum size-dependent proliferation levels. This suggests that, whereas avoidance of cell death simply requires a 'quorum' of small number (2–4) of cells, promoting cell-cycle progression involves greater cooperativity as well as a circuit capable of complex detection of cell density. While detailed biological mechanism(s) for these results remain to be determined, the use of hydrogel microwell-based cellular arrays represents a powerful tool to establish the degree of cellular cooperativity for multiple types of fate decisions.

4. Conclusions

In summary, we developed a new method to systematically investigate multicellular interactions for challenging and motile cells during fate decisions, based on the degree of multicellularity in their microenvironments. The method demonstrated in this study will have general application in the study of multicellular interactions that occur dynamically and result in differentiation, division and cell death. Also, this method can readily be extended for heterogeneous populations of cells by simply labeling each cell type with distinct fluorophore and tracing their fates under their multicellular microenvironments.

Acknowledgments

This work was supported by a grant of the Korea Healthcare technology R&D Project, Ministry for Health, Welfare and Family Affairs (JD, Grant No. A084147), Basic Science Research Program through the National Research Foundation of Korea (NRF) funded by the ministry of Education, Science and Technology (JD, Grant No. 2009-0065183), the POSTECH Basic Science Research Institute Grant (JD), the Sandler Family Foundation (MFK), and grants from the Leukeumia and Lymphoma Foundation and Juvenile Diabetes Research Foundation (MFK). We thank Mary Tang at Stanford Nanofabrication Facility and CIS grant for microfabrication, and Audrey Gerard for critical reading.

Appendix. Supplementary material

Supplementary data associated with this article can be found in the on-line version, at doi:10.1016/j.biomaterials.2010.01.018.

References

[1] Khademhosseini A, Langer R, Borenstein J, Vacanti JP. Microscale technologies for tissue engineering and biology. Proc Natl Acad Sci U S A 2006;103(8):2480–7.
[2] Cordey M, Limacher M, Kobel S, Taylor V, Lutolf MP. Enhancing the reliability and throughput of neurosphere culture on hydrogel microwell arrays. Stem Cells 2008;26(10):2586–94.
[3] Hwang YS, Chung BG, Ortmann D, Hattori N, Moeller HC, Khademhosseini A. Microwell-mediated control of embryoid body size regulates embryonic stem cell fate via differential expression of WNT5a and WNT11. Proc Natl Acad Sci U S A 2009;106(40):16978–83.
[4] Gray DS, Liu WF, Shen CJ, Bhadriraju K, Nelson CM, Chen CS. Engineering amount of cell–cell contact demonstrates biphasic proliferative regulation through RhoA and the actin cytoskeleton. Exp Cell Res 2008;314(15):2846–54.
[5] Nelson CM, Jean RP, Tan JL, Liu WF, Sniadecki NJ, Spector AA, et al. Emergent patterns of growth controlled by multicellular form and mechanics. Proc Natl Acad Sci U S A 2005;102(33):11594–9.
[6] Nelson CM, VanDuijn MM, Inman JL, Fletcher DA, Bissell MJ. Tissue geometry determines sites of mammary branching morphogenesis in organotypic cultures. Science 2006;314(5797):298–300.
[7] Bhatia SN, Balis UJ, Yarmush ML, Toner M. Effect of cell–cell interactions in preservation of cellular phenotype: cocultivation of hepatocytes and nonparenchymal cells. FASEB J 1999;13(14):1883–900.
[8] Nelson CM, Chen CS. Cell–cell signaling by direct contact increases cell proliferation via a PI3K-dependent signal. FEBS Lett 2002;514(2–3):238–42.
[9] Albrecht DR, Underhill GH, Wassermann TB, Sah RL, Bhatia SN. Probing the role of multicellular organization in three-dimensional microenvironments. Nat Meth 2006;3(5):369–75.
[10] Karp JM, Yeh J, Eng G, Fukuda J, Blumling J, Suh KY, et al. Controlling size, shape and homogeneity of embryoid bodies using poly(ethylene glycol) microwells. Lab Chip 2007;7(6):786–94.
[11] Ley K, Laudanna C, Cybulsky MI, Nourshargh S. Getting to the site of inflammation: the leukocyte adhesion cascade updated. Nat Rev Immunol 2007;7(9):678–89.
[12] von Andrian UH, Mackay CR. Advances in immunology: T-cell function and migration – two sides of the same coin. N Engl J Med 2000;343(14):1020–33.
[13] Miller MJ, Wei SH, Parker I, Cahalan MD. Two-photon imaging of lymphocyte motility and antigen response in intact lymph node. Science 2002;296(5574):1869–73.
[14] Bousso P, Robey E. Dynamics of CD8(+) T cell priming by dendritic cells in intact lymph nodes. Nat Immunol 2003;4(6):579–85.
[15] Sabatos CA, Doh J, Chakravarti S, Friedman RS, Pandurangi PG, Tooley AJ, et al. A synaptic basis for paracrine interleukin-2 signaling during homotypic T cell interaction. Immunity 2008;29(2):238–48.
[16] Tang QZ, Adams JY, Tooley AJ, Bi MY, Fife BT, Serra P, et al. Visualizing regulatory T cell control of autoimmune responses in nonobese diabetic mice. Nat Immunol 2006;7(1):83–92.
[17] Wells AD, Gudmundsdottir H, Turka LA. Following the fate of individual T cells throughout activation and clonal expansion – signals from T cell receptor and CD28 differentially regulate the induction and duration of a proliferative response. J Clin Invest 1997;100(12):3173–83.
[18] Kim H, Cohen RE, Hammond PT, Irvine DJ. Live lymphocyte arrays for biosensing. Adv Funct Mater 2006;16(10):1313–23.
[19] Tokilmitsu Y, Kishi H, Kondo S, Honda R, Tajiri K, Motoki K, et al. Single lymphocyte analysis with a microwell array chip. Cytometry A 2007;71A(12):1003–10.
[20] Yamamura S, Kishi H, Tokimitsu Y, Kondo S, Honda R, Rao SR, et al. Single-cell microarray for analyzing cellular response. Anal Chem 2005;77(24):8050–6.
[21] Baskin DS, Ngo H, Didenko VV. Thimerosal induces DNA breaks, caspase-3 activation, membrane damage, and cell death in cultured human neurons and fibroblasts. Toxicol Sci 2003;74(2):361–8.
[22] Han SW, Nakamura C, Obataya I, Nakamura N, Miyake J. Gene expression using an ultrathin needle enabling accurate displacement and low invasiveness. Biochem Biophys Res Commun 2005;332(3):633–9.
[23] Zong WX, Li C, Hatzivassiliou G, Lindsten T, Yu QC, Yuan JY, et al. Bax and Bak can localize to the endoplasmic reticulum to initiate apoptosis. J Cell Biol 2003;162(1):59–69.
[24] Schluter C, Duchrow M, Wohlenberg C, Becker MHG, Key G, Flad HD, et al. The cell proliferation-associated antigen of antibody Ki-67 – a very large, ubiquitous nuclear-protein with numerous repeated elements, representing a new kind of cell cycle-maintaining proteins. J Cell Biol 1993;123(3):513–22.
[25] Suh KY, Park MC, Kim P. Capillary force lithography: a versatile tool for structured biomaterials interface towards cell and tissue engineering. Adv Funct Mater 2009;19(17):2699–712.